Computational Designing Approach for Medium Manganese Steels with Potential Better Hydrogen Embrittlement Resistance

Mahmoud Elaraby [*,], Mohammed Ali [*,**], Mamdouh Eissa [**], Jukka Kömi [*], Pentti Karjalainen [*], Vahid Javaheri [*]**

[*] *Materials and Mechanical Engineering, Centre for Advanced Steels Research, University of Oulu, P.O. Box 4200, FI-90014 Oulu, Finland (e-mail: Mahmoud.elaraby@oulu.fi, mohammed.ali@oulu.fi, jukka.komi@oulu.fi, pentti.karjalainen@oulu.fi, vahid.javaheri@oulu.fi).*

[**] *Steel Technology Department, Central Metallurgical Research and Development Institute, Helwan, 11421, Cairo, Egypt (e-mail: mamdouh.eissa@gmail.com).*

Abstract: Medium manganese steels (MMnS) are known as third-generation high-strength steels, providing an excellent balance of high strength and ductility at a lower cost than those of the second-generation steels. However, the increasing demand for steels with improved hydrogen embrittlement resistance highlights the need for the effective development of new alloys. This study explores the computational design of MMnS with a better combination of strength, ductility, and hydrogen embrittlement resistance. Mechanical properties vary mainly due to changes in chemical composition and processing routes. Computational approaches enable precise optimization of these parameters, avoiding the inefficiencies of traditional trial-and-error. Therefore, CALPHAD-based thermodynamic calculations using Thermo-Calc (TCFE12, MOBFE 7) and JMatPro 14.1 software were employed to design a novel MMnS chemistry, increasing the fraction and stability of the retained austenite and providing efficient traps for hydrogen. As a result, the optimised chemical compositions were determined to be (in wt.%): 0.35C, 9Mn, 1Si, 1Mo, 1 and 3 Al, 0.1Nb, and 0.35C, 9Mn, 1Si, 1Mo, 3Al, 0.05Nb and 0.3V. Thermo-Calc precipitation simulations identified 0.1% Nb as optimal since higher Nb contents reduce carbon in austenite, lowering its stability, and increase the size of the carbides. This Nb content results in NbC formation with an average size distribution around 1 nm, 36 nm, and a size distribution of 1.2×10^{30}, and 5.4×10^{27}respectively. 3% Al promotes the delta ferrite formation and avoids the formation of kappa carbides, and 1% Mo compromises the volume fraction of NbC, strengthening the alloy and serving as an effective hydrogen deep trapping site. 0.3% V was chosen, compromising its effects on the size distribution of VC and available C for the austenitic phase, improving its mechanical stability.

Keywords: Medium Manganese Steels, Hydrogen Embrittlement Resistance, Computational Design, CALPHAD-based Thermodynamic Calculations.

1. INTRODUCTION

Steels with high strength – high ductility, and improved hydrogen embrittlement (HE) resistance have become mandatory in the current era regarding energy applications. The first- generation steels had a relatively high strength but low ductility, which was enhanced in the second-generation steels at the expense of high-cost alloying elements. The third-generation steels, including medium manganese steels (MMnS), compromise the drawbacks of the previous two generations, having better ductility with lower costs (Sun et al., 2023). The physical and mechanical properties of MMnS vary widely depending on alloying elements as well as processing routes (Suh and Kim, 2017). MMnS can have a wide range of chemical compositions (in the following, all concentrations are in wt.%): C 0.01~0.7 (Zhao et al., 2016), Mn 3~12 (Sun et al., 2023), Al 0~10 (Zhao et al., 2016), Si 0~3 (Sun et al., 2018, 2019). Mn is the primary alloying element, and it mainly affects the phase fraction, stability, and morphology of the austenite, defining the mechanical properties and HE resistance. The critical parameter to achieve strength without sacrificing the ductility is retained austenite; that is why it is vital to control its fraction, stability, and morphology achieved by optimal alloying elements, mainly C and Mn content, in addition to processing parameters. Carbon is an austenite stabilizer as it retards the martensitic transformation temperature and decreases the Ae_1 and Ae_3 temperatures. Increasing C content might be beneficial in stabilizing the austenitic phase, though it would deteriorate the weldability, form coarse precipitates, impair the mechanical properties, and lead to intergranular fracture. As indicated by Sun et al. (Sun et al., 2023) Mn serves as the main alloying element as it defines the deformation mechanism by controlling the stacking fault energy (SFE) of the alloys; below 18 mJ/m^2, the transformation-induced plasticity (TRIP) mechanism will be dominating, and higher than 45 mJ/m^2 will activate the dislocation slip, and in the range of 18 to 45 mJ/m^2, will trigger the twinning induced plasticity (TWIP) deformation mechanism. Unlike C, Mn has low diffusivity inside austenite, achieving outstanding mechanical properties through controlling the microstructure via adequate processing parameters of intercritical annealing temperatures and soaking

times (Sun et al., 2016; Ding et al., 2020). Al stabilizes delta ferrite, which was reported to be beneficial for HE resistance for three reasons. First, Al atoms can reduce H diffusivity in austenite due to local expansion around them. Second, enriching the surface oxides prevents H permeation to the alloy. Third, delta ferrite, which Al mainly stabilizes, arrests the propagated cracks, thus retarding failure and enhancing the material toughness. It also has a critical role in controlling the deformation mechanism as it increases the SFE by 8.5 mJ/m^2 (Kang et al., 2012; Lehnhoff et al., 2014). Si addition like Al stabilizes delta ferrite. Wang et al. (Wang et al., 2022a) reported enhancing total elongation (TEL) from 38% to 68% after adding 0.6% Si to 0.2C-6Mn-3Al. Si inhibits cementite precipitation, thereby providing higher carbon content for austenite, enhancing its stability, and reducing dynamic recovery of ferrite, thus increasing the strain hardening rate. Microalloying elements, Mo, Nb, and V, contribute to yield strength and ultimate strength by grain refining and precipitation hardening. They also enhance hydrogen embrittlement resistance; Mo was reported to improve grain boundary cohesion (Yoo et al., 2021) and V and Nb act as active trapping sites for hydrogen (Bhadeshia, 2016).

The traditional methods of achieving required steel properties have been both time-consuming and resource-intensive, underscoring the need for computational approaches in alloy design. Despite their critical importance, studies in this area have been limited, yet the existing research highlights significant benefits. Techniques such as CALPHAD have revolutionized the development of steels by allowing for precise simulations of alloy behaviour and accurate predictions of material outcomes (Patra et al., 2021). These computational methods enhance the efficiency of customizing steel properties, reducing the need for extensive experimental testing. They enable rapid alloy prototyping and optimization, achieving an ideal balance between ductility, strength and cost, and enhancing resistance to HE (Huang et al., 2022).

Despite decades of research (Miller, 1972), industrial production of MMnS with 3–12 Mn still faces significant challenges. These challenges are primarily economic and technical, related to scaling up conventional blast furnace processes, as seen in Voestalpine's trials (Steineder et al., 2019). Alternative electric arc furnaces with argon oxygen decarburizing or vacuum oxygen decarburizing units are necessary but costly. This method also struggles with low Mn recovery and high costs for essential additives such as low-carbon ferromanganese. Processing challenges include maintaining precise control over casting to avoid defects and managing rolling processes to mitigate cracking and other deformities. Weldability issues further complicate MMnS adoption in the automotive industry, with solutions such as introducing nickel interlayers in welds proposed to enhance joint quality (DiGiovanni et al., 2021). Advancements in process optimization, cost efficiency, and microstructural control are crucial to moving MMnS toward commercial viability. Transitioning from pre-commercial stages to total industrial production may take about ten years. This process will require cooperation among steelmakers, automotive manufacturers, and researchers to create viable and cost-effective solutions for broad implementation.

The present study utilized different modules of Thermo-Calc and JMatPro to optimize the alloy's chemical composition. The aim was to increase the fraction and stability of retained austenite by optimizing annealing temperature and time, thereby improving mechanical properties and enhancing HE resistance.

2. METHODOLOGY

The CALPHAD methodology employs Thermo-Calc and JMatPro to design steel alloys by optimizing the effects of alloying elements such as C, Mn, Al, Si, Mo, Nb, and V. Annealing temperatures ranged from 500–800°C, with a total of 2,880 alloy compositions assessed, as detailed in Table 1. Specifically, Thermo-Calc (TCFE 12, MOBFE 7) utilized the TC and PRISMA modules. These modules facilitated the simulation of the effect of alloying on the characteristics of the austenitic phase, including the martensite start temperature Ms and the austenite volume fraction. These parameters were studied to obtain optimal retained austenite fraction and stability as well. Moreover, the PRISMA module, which employs the Langer-Schwartz theory (Langer and Schwartz, 1980) and the Kampmann-Wagner (Wagner et al., 2001) numerical method to simulate the nucleation, growth, and coarsening of precipitates in multi-component systems, was used to simulate the precipitation behaviour (Chen et al., 2014). This includes predictions of the mean size of precipitates, volume fraction, size distribution, and the contribution of precipitation strengthening to the yield strength, considering varying alloy compositions with temperature and time. This extension of classical nucleation theory enables accurate modelling of real system precipitations based on appropriate thermodynamic and kinetic databases. Furthermore, JMatPro was utilized to investigate the alloy's mechanical and physical properties through the solidification, thermo-physical properties, and phase transformation modules, thereby analysing the diffusion of elements over time and the effect of cooling rates on phase formation. This integrative approach underscores the pivotal role of computational tools in advancing our understanding and development of high-performance steel alloys. The simulation graphs were made to study the effects of alloying elements using 0.35C-9Mn-1Si-1Mo-3Al-0.1Nb (with designated code 310) and 0.35C-9Mn-1Si-1Mo-3Al-0.05Nb-0.3V (with designated code 353) where the numbers represent Al, Nb, and V respectively.

3. RESULTS AND DISCUSSION

3.1 Carbon

Carbon is one of the main alloying elements in MMnS; it affects the volume fraction and stability of austenite as well as the formation temperature of precipitates and their fraction. The effect of carbon on the austenite volume fraction, shown in Fig. 1, can be divided into two distinct stages. In the first stage, the austenite fraction exhibits a parabolic curve with increasing temperature, indicating a progressive increase until the cementite particles are completely dissolved, as seen from Fig. 2. In the subsequent stage, the rate of increase in the austenite volume fraction follows a linear relationship with temperature, as seen in Fig. 1. Cementite formation greatly

Table 1 Range of alloy compositions (wt.%) used in the simulation for optimizing the chemical composition.

	Lower limit	Upper limit	Step
Temperature (°C)	500	800	2
C	0.1	0.4	0.1
Mn	7	11	1
Si		1 (constant)	
Al	1	3	1
Mo	0.5	2	0.5
Nb	0.05	0.2	0.05
V	0.2	0.4	0.1
Fe		balance	
Total number of alloys		2880	

affects the austenite volume fraction due to the reduction of carbon and manganese contents.

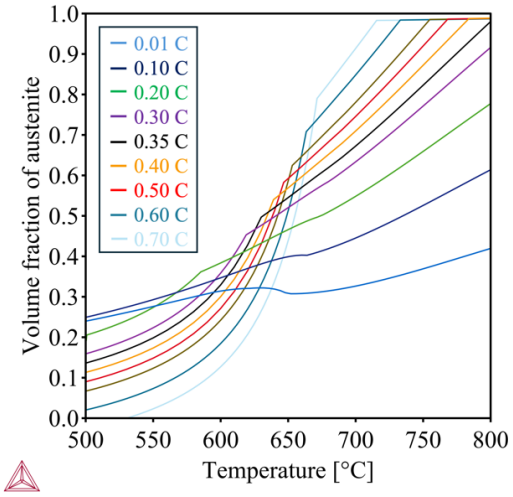

Fig. 1 Effect of carbon content on the austenite volume fraction in the temperature range of 500-800ºC for alloy 310.

Increasing the carbon content to some extent not only enhances the ultimate strength due to the transformed hard martensitic phase and induces high dislocation density to the soft ferritic phase through the TRIP effect (Ennis et al., 2017) but also improves the material's ductility by increasing the mechanical stability of austenite, enabling it to accommodate more strain during the progressive work hardening thereby retarding the necking (localization of deformation) and enhancing homogeneous deformation (Zou et al., 2021). Below 0.2% C, the carbon content is relatively low, and so is the austenite volume fraction, as shown in Fig. 1; above 0.40% C, it would negatively impact the toughness due to the formation of brittle phases like cementite. At these levels, there is also a risk of reduced weldability and increased susceptibility to cracking under stress (Bhattacharya et al., 2019). A range of 0.2–0.4% C was selected to compromise the austenite volume fraction and stability. Regarding the studied effect of 0.2–0.4% C on the ultimate tensile strength and martensite start temperature Ms with annealing time that represents the austenite stability shown in Fig. 3. It is seen that 0.35% C shows a reliable austenite stability.

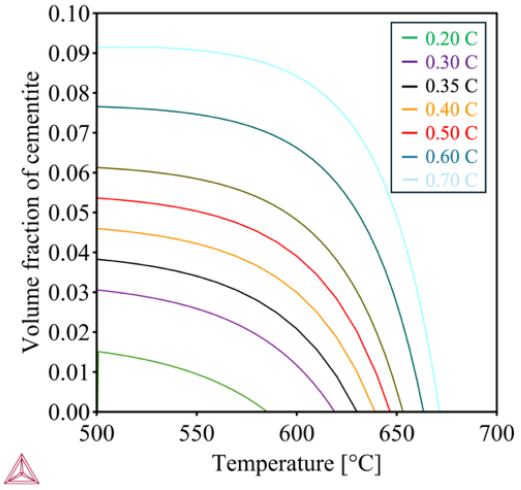

Fig. 2 Effect of carbon content on cementite´s formation temperature and fraction, alloy 310.

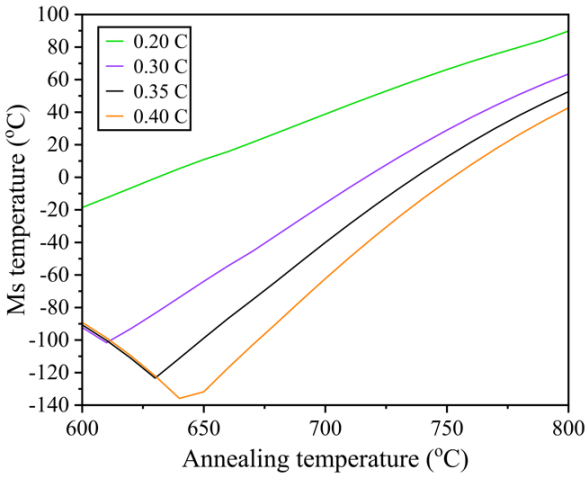

Fig. 3 Effect of carbon content on Ms temperature of intercritically annealed austenite at different annealing temperatures.

3.2 Manganese

Manganese is the key role element in MMnS stabilizing austenite phase and controlling the deformation mechanism through manipulating the SFE to activate both TRIP+TWIP mechanisms so that the material can accommodate higher strain levels without the deformation localization resulting in material fracture and improving both yield strength through grain refining of twinning effect and enhanced ultimate tensile strength by the TRIP effect. Previous studies have shown outstanding mechanical properties for Mn content 7–11%. (Sun et al., 2023; Zhang et al., 2024), reaching a product of strength and elongation (PSE) of 64 GPa% (Luo and Dong, 2016) for 9% Mn. Increasing Mn content will increase the fraction of the austenitic phase, reducing C content due to the dilution effect and suppressing the formation of carbides such as cementite by preferentially stabilizing carbon in the austenite phase, as shown in Figs. 4 and 5.

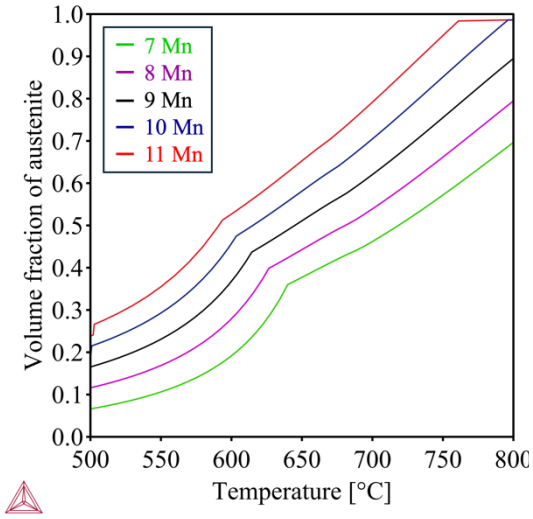

Fig. 4 Effect of Mn content on austenite volume fraction within the 500–800 °C temperature range, alloy 310.

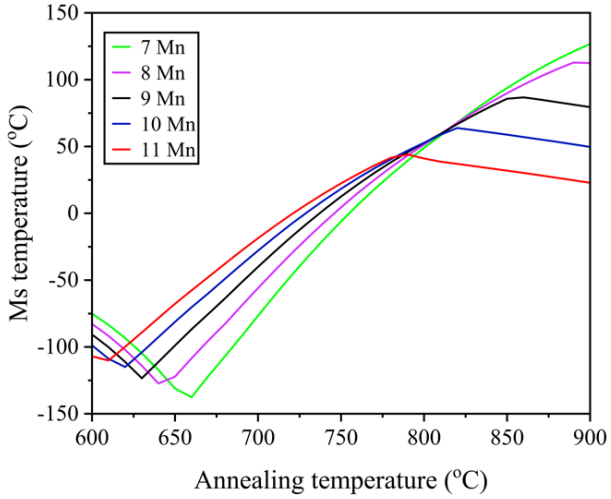

Fig. 5 Effect of Mn content on Ms temperature, alloy 310.

This suppression is beneficial for retaining ductility and toughness, as excessive cementite can embrittle the steel (Kozłowska et al., 2019). Austenite stability is affected by both C and Mn content; austenite stability is highest (lowest Ms temperature) when C content reaches its maximum value, then austenite stability increases (Ms decreases) to its minimum due to the increased carbon content resulting from cementite dissolution, then with increasing annealing temperature stability decreases (Ms increases) due to dilution effect (increased austenite volume fraction) till it is completely austenite (Ac_3) as shown in Figs. 5 and 6. Optimizing austenite volume fraction, stability (represented by Ms), and alloying addition cost; 9% Mn was chosen for the alloys.

3.3 Silicon and Aluminum

Previous studies showed that 1–3% Al does not form delta ferrite, while 3–5% Al is high enough to obtain delta ferrite, but more than 5% results in kappa-carbide formation as shown in Fig. 7. Hence, it is critical to have the proper Al content for obtaining delta ferrite and avoid formation of kappa-carbide, which would deteriorate the mechanical properties (Zhang et al., 2024). Al stabilizes ferrite and increases SFE per 8.5 mJ/m^2 by 1%, which is beneficial for controlling the deformation mechanism (Sun et al., 2023), resulting in improved HE resistance through reducing the fraction of transformed martensite (Ryu et al., 2013). Al can affect the mechanical stability of austenite due to the heterogeneity of Mn content in austenite. This is explained by the slower velocity of interface movement, which decreases from (1.54×10^{-11} to 7.24×10^{-12} m s^{-1}), with the addition of (~2% Al). Consequently, there is a successive austenite to martensite transformation from regions of a low Mn content to those of a higher Mn content. This transformation improves the material strength without losing material toughness (Ye et al., 2022). Al was reported to reduce HE (Koyama et al., 2017) through two possible mechanisms: first, the strain field around Al atoms, acting as weak trapping sites, reduces the diffusion of hydrogen atoms (Han et al., 2015; Song et al., 2014), and secondly, it reduces hydrogen permeation in the material by enriching surface oxides (Park et al., 2012).

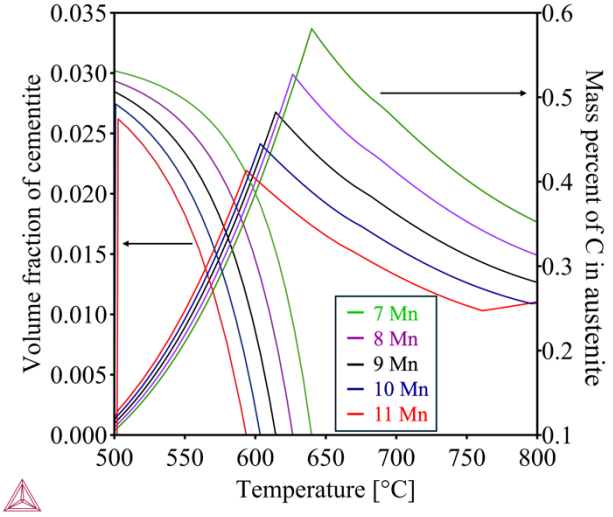

Fig. 6 Effect of Mn content on cementite fraction, formation temperature, and C in austenitic phase, alloy 310.

Two levels of Al, 1% and 3%, were chosen to study their effect on mechanical properties, the formation of delta ferrite, and the HE resistance.

Si has a similar effect to Al as it restrains cementite formation, thereby providing enough C content for austenite stabilization (Kwok and Dye, 2023). The addition of Si also reduces the dynamic recovery of ferrite, thus increasing the strain-hardening rate (Ma, 2017). It was reported that adding 0.6%Si enhanced TEL by 30% and enhanced the HE resistance as well (Wang et al., 2022b). In another study, effects of 0, 1, and 3 Si were studied in 0.2C-10Mn-3Al alloy, and it was found that 1% Si showed enhanced TEL, ultimate strength, and work hardening rate that can be attributed to the strain partitioning between austenite and ferrite. This was the main reason for the higher and uniform TEL and higher work hardening rate in 1 Si, unlike in 3 Si, where no strain partitioning was noticed. Regarding the literature survey, the alloys with 1% Si content was selected.

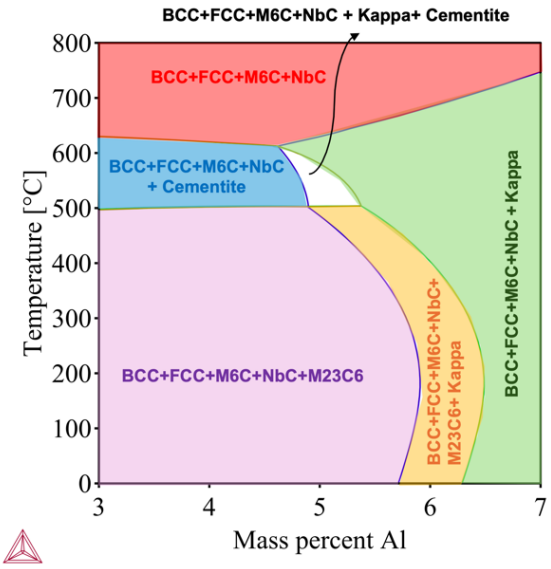

Fig. 7 Effect of Al content on kappa carbide formation, alloy 310.

3.4 Niobium and Molybdenum

Niobium exists in steel in two forms: the first and most familiar one is the carbide/carbonitride form, as Nb has a high affinity for carbon, and the second one is as a solid solution in the matrix, which can be achieved through proper processing routes (Ali et al., 2024). Both forms improve steel mechanical properties at high temperatures through the drag effect of Nb by inhibiting grain growth. At relatively low temperatures, grain growth is hindered, and hydrogen embrittlement resistance is enhanced by the pinning effect of NbC particles, which act as an active trapping site for hydrogen (Wei and Tsuzaki, 2012).

Wang et al. (Wang et al., 2010) investigated the influence of Mo on the formation and morphology of NbC and VC precipitates in steel. Their study revealed that the addition of Mo led to a reduction in the size of NbC precipitates, attributed to the segregation of Mo at the carbide/matrix interface. This segregation impedes the diffusion of Nb and V atoms from the matrix into the carbide phase and retards the diffusion kinetics of carbon and the alloying elements within the matrix. Consequently, the growth of the NbC and VC particles is significantly suppressed. The hydrogen trapping capacity of VC, NbC, and TiC was investigated through thermal desorption spectroscopy, and NbC was reported to have the largest trapping capacity (Wei and Tsuzaki, 2012). NbC was reported to have a beneficial effect on reducing the number of Σ3 boundaries, which reduces hydrogen-induced cracking (HIC) resistance (Zhang et al., 2018), and increasing the Σ11 boundaries, which increases the HIC resistance (Venegas et al., 2009). In an investigation on the effect of Nb and/or Mo addition on retained austenite volume fraction, stability, and hydrogen embrittlement resistance, the combined addition of Nb and Mo was found to result in the highest austenite volume fraction and stability (lowest Ms temperature) with the best HE resistance (Luo et al., 2022). Various empirical studies (Geng et al., 2000, 2001) using first-principles full-potential linearized augmented plane-wave method calculations were performed to investigate the effect of elements on Fe Σ3 grain boundary cohesion, revealing that Nb and Mo have embrittling values ΔE_B^A(eV) -1.24 and -0.96 (lower is better) respectively. The effect of Mo on Σ3 boundary was experimentally investigated (Yoo et al., 2021) to confirm the positive effect of Mo on enhancing grain cohesion and HE resistance. Precipitation of NbC was simulated using PRISMA. The results showed that 0.10 Nb is the optimal content as 0.05 and 0.2 have larger particle size and lower number density than 0.10 Nb as shown in Fig. 8. Increasing the Nb content increases the volume fraction of NbC as shown if Fig. 9. It was reported that a larger number of carbides with smaller sizes is more effective for trapping hydrogen atoms (Liu et al., 2024). While increasing Mo content has a beneficial effect on increasing the volume fraction of NbC and lowering its size, as mentioned before, it also has a negative effect on the austenite as it reduces the austenite volume fraction by reducing the available carbon, which stabilizes the austenite as illustrated in Fig. 10.

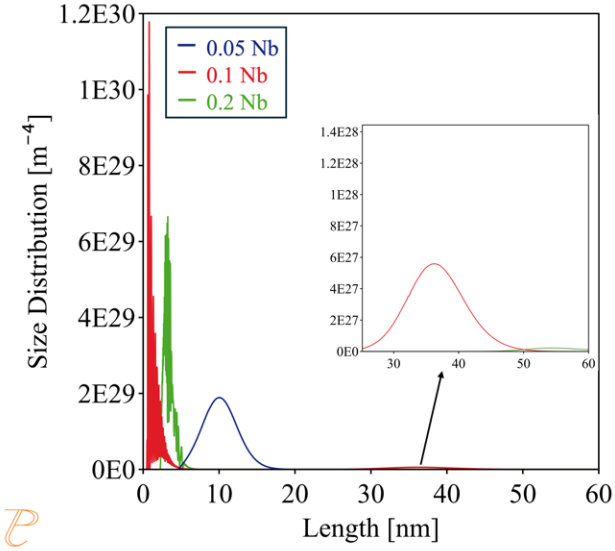

Fig. 8 Effect of Nb content on size distribution on NbC, alloy 310.

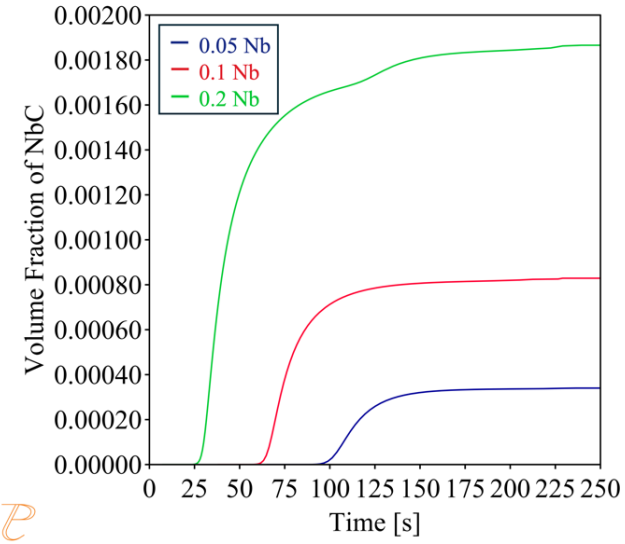

Fig. 9 Effect of Nb content on volume fraction of NbC, alloy 310.

3.5 Vanadium

The effect of V content on austenite stability through its impact on C in the austenitic phase was simulated in Fig. 11, showing that increasing V content leads to a decrease in the available C of the austenitic phase, resulting in lower stability, thus deteriorating the HE resistance. On the other hand, increasing the V content from 0.2% to 0.4% increases the size distribution of VC from 4.8 × 10^{30} to 3.4 × 10^{31}, as shown in Fig. 12, enhancing the HE resistance. Compromising the effects of V content on austenite stability and size distribution of VC, 0.3% V was chosen along with 0.05% Nb to obtain C content high enough to increase austenite stability and nano-carbide precipitates for improving both mechanical properties and HE resistance.

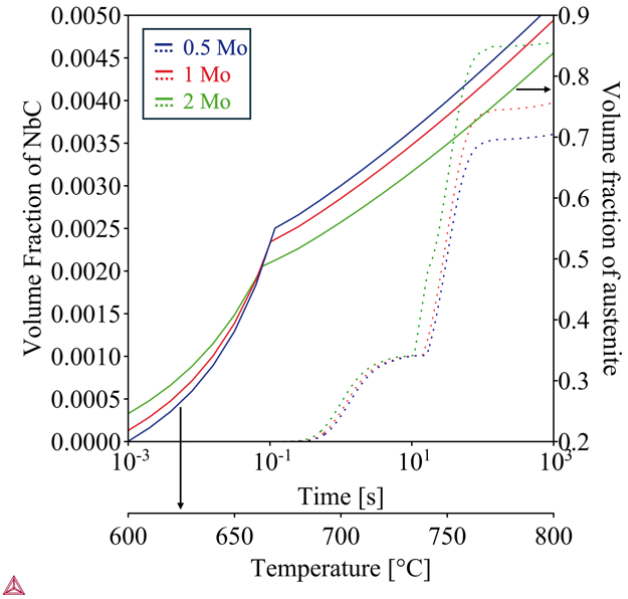

Fig. 10 Effect of Mo on precipitation of NbC and austenite volume fraction, alloy 310.

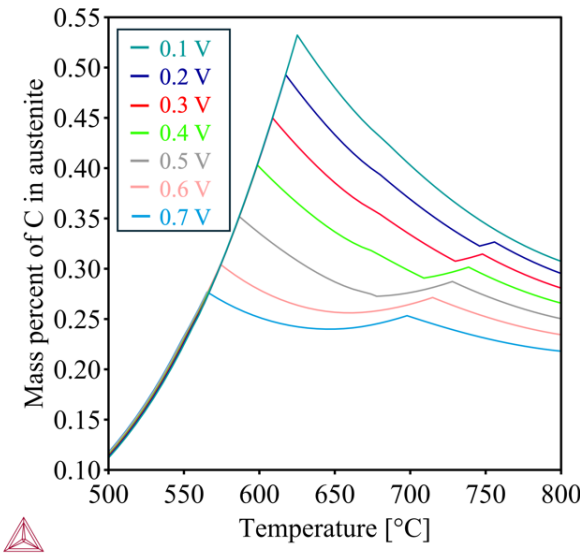

Fig. 11 Effect of V content on C concentration in austenite, alloy 353.

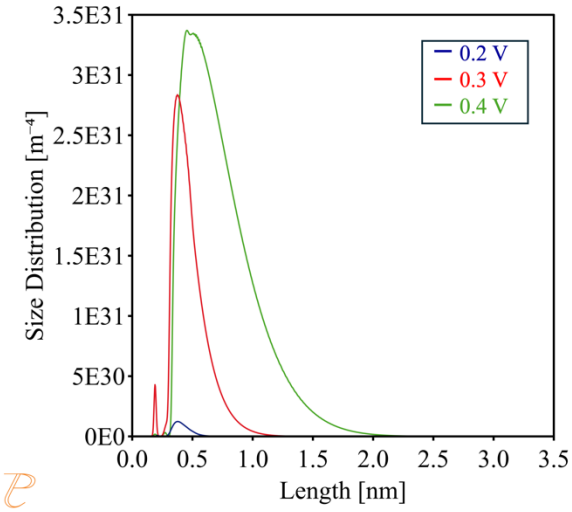

Fig. 12 Effect of V content on the size distribution of VC, alloy 353.

4. CONCLUSIONS

This study presents a comprehensive computational design approach for medium manganese steels aimed at enhancing mechanical properties and hydrogen embrittlement resistance. Through CALPHAD-based thermodynamic calculations and JMatPro simulations, we optimized the chemical composition to achieve a balance of high strength, ductility, and resistance to hydrogen embrittlement, as illustrated in the flow chart in Fig. 13.

Key findings include:

Optimized Composition: The optimized chemical compositions, consist of (in wt.%):

1. 0.35C, 9Mn, 1Si, 1Mo, with variations of 1 and 3 Al, and 0.1 Nb.
2. 0.35C, 9Mn, 1Si, 1Mo, 3 Al, 0.05 Nb and 0.3 V.

as optimal for enhancing mechanical properties and hydrogen embrittlement resistance.

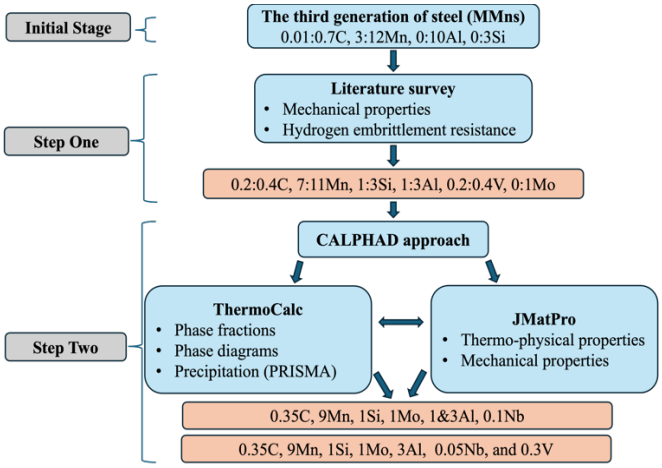

Fig. 13. Flow chart for computational designing approach for medium manganese steels with potential better hydrogen embrittlement resistance.

Role of Alloying Elements:

Carbon (C): A 0.35% C was found to provide a reliable strengthening effect and austenite stability.

Manganese (Mn): 9% Mn stabilizes the austenitic phase, enabling both TRIP and TWIP deformation mechanisms, which enhances ductility and strength.

Silicon (Si) and Aluminum (Al): Both elements help to stabilize the ferritic phase and control the deformation mechanism, with 1% Si and 1 and 3% Al being particularly effective.

Niobium (Nb): 0.1% Nb was optimal for forming fine NbC precipitates with high number density, which improve strength and serve as hydrogen deep trapping sites.

Molybdenum (Mo): 1% Mo was effective in refining the NbC precipitate size and increasing its volume fraction, further enhancing strength and hydrogen embrittlement resistance.

Vanadium (V): 0.3% V provides a balanced austenite stability and carbide size distribution, improving mechanical properties and hydrogen embrittlement resistance.

ACKNOWLEDGMENTS

The authors would like to thank Jane ja Aatos Erkko Foundation and Tiina and Antti Herlin Foundation for their financial supports on Advanced Steels for Green Planet project. Mohammed Ali would like to acknowledge the financial support of Interreg Aurora, project Sustainable Hydrogen - Potential for Bothnia Gulf Cluster, project number 20357962.

REFERENCES

Ali, M., Alatarvas, T., and Kömi, J. (2024). Impact of niobium addition and non-metallic inclusions' characteristics on the microstructure and mechanical properties of low-carbon CrNiMnMoB ultrahigh-strength steel: A comprehensive investigation. Journal of Materials Research and Technology, 30, 6133–6153.

Bhadeshia, H. K. D. H. (2016). Prevention of hydrogen embrittlement in steels. ISIJ International, 56(1), 24–36.

Bhattacharya, A., Bokinala, P. K., Mitra, R., and Chakrabarti, D. (2019). Relative effect of C and Mn on strength-toughness of medium Mn steels. Materials Science and Technology, 35(1), 55–67.

Chen, Q., Wu, K., Sterner, G., and Mason, P. (2014). Modeling precipitation kinetics during heat treatment with Calphad-based tools. Journal of Materials Engineering and Performance, 23(12), 4193–4196.

Ennis, B. L., Jimenez-Melero, E., Atzema, E. H., Krugla, M., Azeem, M. A., Rowley, D., Daisenberger, D., Hanlon, D. N., and Lee, P. D. (2017). Metastable austenite driven work-hardening behaviour in a TRIP-assisted dual phase steel. International Journal of Plasticity, 88, 126–139.

DiGiovanni, C., Ghatei Kalashami, A., Goodwin, F., Biro, E, and Zhou, N. Y. 2021. Occurrence of sub-critical heat affected zone liquid metal embrittlement in joining of advanced high strength steel. Journal of Materials Processing Technology, 288:116917.

Geng, W. T., Freeman, A. J., and Olson, G. B. (2001). Influence of alloying additions on grain boundary cohesion of transition metals: First-principles determination and its phenomenological extension. Physical Review B, 63, 165415.

Geng, W. T., Freeman, A. J., Wu, R., and Olson, G. B. (2000). Effect of Mo and Pd on the grain-boundary cohesion of Fe. Physical Review B, 62(10), 6208.

Huang, C., Hu, C., Liu, Y., Liang, Z., and Huang, M. (2022). Recent developments and perspectives of advanced high-strength medium Mn steel: from material design to failure mechanisms. Materials Futures, 1(3), 032001.

Kang, M., Woo, W., Lee, Y. K., and Seong, B. S. (2012). Neutron diffraction analysis of stacking fault energy in Fe–18Mn–2Al–0.6C twinning-induced plasticity steels. Materials Letters, 76, 93–95.

Kozłowska, A., Janik, A., Radwański, K., and Grajcar, A. (2019). Microstructure evolution and mechanical stability of retained austenite in medium-Mn steel deformed at different temperatures. Materials, 12(18), 3042.

Kwok, T. W. J., and Dye, D. (2023). A review of the processing, microstructure and property relationships in medium Mn steels. International Materials Reviews, 68(8), 1098– 1134.

Langer, J. S., and Schwartz, A. J. (1980). Kinetics of nucleation in near-critical fluids. Physical Review A, 21(3), 948.

Lehnhoff, G. R., Findley, K. O., and De Cooman, B. C. (2014). The influence of silicon and aluminum alloying on the lattice parameter and stacking fault energy of austenitic steel. Scripta Materialia, 92, 19–22.

Liu, P. Y., Zhang, B., Niu, R., Lu, S. L., Huang, C., Wang, M., Tian, F., Mao, Y., Li, T., Burr, P. A., Lu, H., Guo, A., Yen, H. W., Cairney, J. M., Chen, H., and Chen, Y. S. (2024). Engineering metal-carbide hydrogen traps in steels. Nature Communications, 15(1), 1–13.

Luo, H. and Dong, H. (2016). CN106119493B.

Luo, Y., Lu, H., Min, N., Li, W., and Jin, X. (2022). Effect of Mo and Nb on mechanical properties and hydrogen embrittlement of hot-rolled medium-Mn steels. Materials Science and Engineering: A, 844, 143108.

Ma, Y. (2017). Medium-manganese steels processed by austenite-reverted-transformation annealing for automotive applications. Materials Science and Technology (United Kingdom), 33(15), 1713–1727.

Miller, R. L. (1972). Ultrafine-grained microstructures and mechanical properties of alloy steels. Metallurgical Transactions, 3(4), 905–912.

Park, I. J., Jeong, K. H., Jung, J. G., Lee, C. S., and Lee, Y. K. (2012). The mechanism of enhanced resistance to the hydrogen delayed fracture in Al-added Fe–18Mn–0.6C twinning-induced plasticity steels. International Journal of Hydrogen Energy, 37(12), 9925–9932.

Patra, A. K., Athreya, C. N., Mandal, S., Hari Kumar, K. C., and Subramanya Sarma, V. (2021). High strength-high ductility medium Mn steel obtained through CALPHAD based alloy design and thermomechanical processing. Materials Science and Engineering: A, 810, 140756.

Ryu, J. H., Kim, S. K., Lee, C. S., Suh, D. W., and Bhadeshia, H. K. D. H. (2013). Effect of aluminium on hydrogen-induced fracture behaviour in austenitic Fe–Mn–C steel. Proceedings of the Royal Society A: Mathematical, Physical and Engineering Sciences, 469, 2149.

Steineder, K., Daniel K., Schickinger, M., Thomas Hebesberger, T., and Schneider, R. (2019). Wärmebehandlungsoptionen von Medium-Mn-Stählen für den (Automobil) Leichtbau. BHM Berg- und Hüttenmännische Monatshefte, 164(9), 379–384.

Suh, D. W., and Kim, S. J. (2017). Medium Mn transformation-induced plasticity steels: Recent progress and challenges. Scripta Materialia, 126, 63–67.

Sun, B., Fazeli, F., Scott, C., Brodusch, N., Gauvin, R., and Yue, S. (2018). The influence of silicon additions on the deformation behavior of austenite-ferrite duplex medium manganese steels. Acta Materialia, 148, 249–262.

Sun, B., Fazeli, F., Scott, C., and Yue, S. (2016). Phase transformation behavior of medium manganese steels with 3 Wt Pct aluminum and 3 Wt Pct silicon during intercritical annealing. Metallurgical and Materials Transactions A: Physical Metallurgy and Materials Science, 47(10), 4869–4882.

Sun, B., Kwiatkowski da Silva, A., Wu, Y., Ma, Y., Chen, H., Scott, C., Ponge, D., and Raabe, D. (2023). Physical metallurgy of medium-Mn advanced high-strength steels. International Materials Reviews, 68(7), 786–824.

Sun, B., Liu, G., He, J., Li, T., Wan, X., Dai, Z., Ponge, D., Raabe, D., Zhang, C., Godfrey, A., Miyamoto, G., Furuhara, T., Yang, Z., van der Zwaag, S., and Chen, H. (2020). Chemical boundary engineering: A new route toward lean, ultrastrong yet ductile steels. Science Advances, 6(13), eaay1430.

Sun, B., Palanisamy, D., Ponge, D., Gault, B., Fazeli, F., Scott, C., Yue, S., and Raabe, D. (2019). Revealing fracture mechanisms of medium manganese steels with and without delta-ferrite. Acta Materialia, 164, 683–696.

Venegas, V., Caleyo, F., Baudin, T., Hallen, J. M., and Penelle, R. (2009). Role of microtexture in the interaction and coalescence of hydrogen-induced cracks. Corrosion Science, 51(5), 1140–1145.

Wagner, R., Kampmann, R., and Voorhees, P. W. (2001). Homogeneous second-phase precipitation. Phase Transformations in Materials, 309–407.

Wang, Z., Wan, Z., Chen, X., Xu, J., Zhou, Y., Huang, T., Kong, X., Ou, C., Zhang, J., and Li, J. (2022b). The H-induced fracture behavior in hot rolled medium Mn steels with and without δ-ferrite. Engineering Failure Analysis, 141, 106651.

Wang. Z., Zhu, X., and Liu. W. (2010). Influence of Mo on tempering precipitation in Nb–Mo–V microalloyed steels. Chinese Journal of Materials Research. 24(2) 217–222.

Wei, F. G., and Tsuzaki, K. (2012). Hydrogen trapping phenomena in martensitic steels. In Gaseous Hydrogen Embrittlement of Materials in Energy Technologies: The Problem, its Characterisation and Effects on Particular Alloy Classes (Vol. 2, pp. 493–525). Woodhead Publishing.

Ye, Q., Yu, Y., Zhu, H., Li, J., Qiao, L., and Yan, Y. (2022). Formation of core-shell austenite as promoted by alloying solutes in hot-rolled medium Mn steel. Journal of Materials Research and Technology, 21, 1053–1060.

Yoo, J., Jo, M. C., Jo, M. C., Kim, S., Kim, S. H., Oh, J., Sohn, S. S., and Lee, S. (2021). Effects of solid solution and grain-boundary segregation of Mo on hydrogen embrittlement in 32MnB5 hot-stamping steels. Acta Materialia, 207, 116661.

Zhang, Y., Ye, Q., and Yan, Y. (2024). Processing, microstructure, mechanical properties, and hydrogen embrittlement of medium-Mn steels: A review. Journal of Materials Science & Technology, 201, 44–57.

Zhao, C., Song, R., Zhang, L., Yang, F., and Kang, T. (2016). Effect of annealing temperature on the microstructure and tensile properties of Fe–10Mn–10Al–0.7C low-density steel. Materials & Design, 91, 348–360.

Zou, Y., Ding, H., and Tang, Z. (2021). Effect of carbon content on deformation behavior and partitioning of manganese in medium-Mn steels. Metals, 11(4), 667.